

Self-modulated wakefield and forced laser wakefield acceleration of electrons^{a)}

Z. Najmudin,^{b)} K. Krushelnick, E. L. Clark, S. P. D. Mangles, B. Walton, and A. E. Dangor
Blackett Lab., Imperial College, London SW7 2BZ, United Kingdom

S. Fritzler and V. Malka
Laboratoire d'Optique Appliquée, ENSTA, École Polytechnique, CNRS, 91761 Palaiseau, France

E. Lefebvre
*Département de Physique Théorique et Appliquée, CEA/DAM Ile-de-France, BP12,
 91680 Bruyères-le-Châtel, France*

D. Gordon
Plasma Physics Division, Naval Research Laboratory, Washington, DC 20375

F. S. Tsung and C. Joshi
University of California, Los Angeles, California 90095

(Received 13 November 2002; accepted 5 February 2003)

The interaction of intense laser pulses (power > 30 TW) with underdense plasmas has been studied. In the regime where the pulse length is much longer than the plasma period ($\tau_l \gg 2\pi\omega_p^{-1}$), the laser pulse is found to be self-modulated at the plasma frequency by the forward Raman scattering instability. Wavebreaking of the resulting plasma wave results in energetic electrons being accelerated to more than 100 MeV. Reducing the pulse length so that $\tau_l \sim 2\pi\omega_p^{-1}$, but retaining the same power, also leads to wavebreaking. This is a direct result of a combination of laser beam self-focusing, front-edge laser pulse steepening and relativistic lengthening of the plasma wave wavelength, which can result in a forced growth of the wakefield plasma wave, even for initially nonresonant laser pulses ($\tau_l \neq \pi\omega_p^{-1}$). Since, in this forced laser wakefield regime, the interaction of the plasma wave and the bunch of accelerated electrons with the laser pulse is reduced, this can result in higher energy gain (to beyond 200 MeV) and better beam quality. © 2003 American Institute of Physics. [DOI: 10.1063/1.1564083]

I. INTRODUCTION

Great interest has been aroused by the prospect of using lasers to accelerate particles, in particular electrons, to extremely high energies.¹ Though state-of-the-art lasers can have incredibly high intrinsic electric fields ($E_0 \approx 6 \text{ TV m}^{-1}$ for $I_0 = 1 \times 10^{19} \text{ W cm}^{-2}$), these electric fields are transverse and oscillating, meaning that they cannot be used for longitudinal acceleration over many laser cycles. It has been proposed that the generation of plasma waves through the action of the laser's ponderomotive force is an ideal way of converting the power of these modern lasers into a longitudinal electric field with relativistic phase velocity.² In this paper we show two specific regimes of laser-plasma wave interaction, which can lead to the development of these accelerating structures. In both cases it will be shown that the power of the laser can be sufficient to lead to nonlinear steepening of the plasma wave and eventually to wavebreaking.

In the self-modulated wakefield regime (SMWF),^{3,4} a laser pulse with pulse duration τ_l much greater than the inverse plasma frequency ω_p^{-1} , is severely modulated at the plasma frequency by the nonlinear interaction of the plasma wave.

The process can be considered a quasi-quantum coupling of the photons (frequency ω_0) with plasmons ($\omega = \omega_p$), to give scattered photons at frequencies $\omega_0 \pm \omega_p$. The resulting beating of the driver and scattered photons modulates the laser pulse amplitude at ω_p . Through the action of the ponderomotive force, this plasma frequency modulation can result in the resonant growth of the plasma wave that initiated the scattering. Direct forward scattering (so that the scattered photons stay in the same direction as the original laser beam) has a relatively slow growth rate, which saturates at relativistic intensities (i.e., where the normalized momentum a_0 of electron quiver in the laser field approaches 1).⁵ Scattering at angles away from the z -direction (the propagation direction of the laser), has higher growth rates,^{6,7} but shorter growth lengths. However, it does play an important role in the growth of the forward scattering instabilities, since the initial growth of these instabilities can be so large for $a_0 \sim 1$ that they can erode the front of the laser pulse dramatically, thus forming a sharp intensity gradient.^{8,9} This can impulsively set up a much larger amplitude noise source from which the direct forward scattering can grow. This allows a self-modulated laser pulse to generate plasma waves of amplitude close to the initial plasma density on time scales of the order of ~ 1 ps or less. Since the characteristic of this interaction is the production of satellite frequencies of spacing $n \cdot \omega_p$

^{a)}Paper FI2 3, Bull. Am. Phys. Soc. **47**, 94 (2002).

^{b)}Invited speaker. Electronic mail: zn1@ic.ac.uk

(where n is an integer) from the original laser frequency, this process is often called stimulated Raman scattering, in analogy to the scattering from virtual excited states of molecules.

The pulse erosion at the leading edge can become so severe for sufficiently high intensity pulses, that most of the plasma wave growth eventually occurs there. In this case, the plasma wave growth becomes very similar to the growth in the nonlinear wakefield regime, and takes place in a time less than $\pi\omega_p^{-1}$. It can be supposed that it may, in this case, be much more efficient to use a laser pulse of pulse length shorter than this time. Despite the incredible reduction in pulse durations now achieved with ultrahigh power laser systems, it is still difficult to directly generate a pulse with rise times sufficiently short to generate plasma waves at a suitable density. However, even in the regime where the pulse is still long compared to the plasma period, if the pulse is sufficiently intense, then through its nonlinear interaction with the plasma, it can still experience leading edge pulse compression resulting in the required fast rise time. This is due to the nonlinear interaction of the rising edge of the pulse with the plasma wake pushed in front of the laser pulse by its ponderomotive force. The growing plasma wave retards the very front of the laser pulse, so compressing it.¹⁰ The increasing density due to ionization by the laser pulse will also contribute in a similar manner.¹¹ This optical compression in conjunction with the nonlinear wavelength increase of the plasma wave as its amplitude increases [for $a_0 > 1$, $\lambda_{NL} = (2/\pi)(1 + (a_0^2/2))^{1/2}\lambda_p$, where $\lambda_p = 2\pi c/\omega_p$], can result in a highly efficient growth of the plasma wave, even in the case where the pulse length of the laser is initially longer than the plasma period.¹² This nonresonant excitation of the plasma wave has been termed a forced laser wakefield (FLW) excitation.¹³

The nonlinear response of the plasma as the plasma wave amplitude grows to the order of the initial plasma density n_0 also results in steepening of the plasma wave. Indeed the density spikes can have an amplitude $\delta n > n_0$. The electric field associated with this plasma wave can thus be greater than the maximum electric field associated with a linear plasma wave $E_0 = m_e c \omega_p / e$, and can thus result in ultrahigh accelerating gradients. In the nonlinear wakefield regime,^{14,15} the maximum longitudinal electric field is given as $E_{\max} = ((a_0^2/2)/\sqrt{1 + (a_0^2/2)})E_0$ for linear polarized light. Hence for $a_0 \gg 1$, one can see that the electric field, and hence the plasma wave amplitude, approaches the (nonlinear) cold wavebreaking limit¹⁶ $E_{wb} = \sqrt{2}(\gamma_p - 1)^{1/2}E_0$, where $\gamma_p = (1 - (v_p/c)^2)^{-1/2}$ is the Lorentz factor associated with the relativistic plasma wave, which for sufficiently underdense plasma can be approximated by $\gamma_p \approx \omega_0/\omega_p$. One can see that these accelerating fields are huge, approaching 1 TV m^{-1} , for plasma densities around $n_e = 1 \times 10^{19} \text{ cm}^{-3}$. In addition, these accelerating structures travel with the laser pulse and so have a relativistic factor γ equal to that of the laser pulse in the plasma γ_p . Hence they can accelerate a relativistic particle, which can stay in phase with the accelerating field, to extremely high energies.

Indeed if the E -field of the plasma waves does approach E_{wb} , then the process of wavebreaking can provide the electrons to be accelerated.¹⁷ Wavebreaking, which sets the lim-

iting electric field, occurs because some of the plasma electrons undergo such large oscillations that the returning force due to the plasma wave is no longer large enough to make them continue their longitudinal oscillation. Instead the electrons can continue into the next wave "bucket." If this is the forward traveling "bucket," then the electron will feel a continued acceleration, so resulting in its trapping within the plasma wave. The trapped electrons continue to be accelerated until their velocity exceeds that of the plasma wave and they "out-run" the wave and are dephased. The maximum energy gain before electrons "out-run" the accelerating field (ignoring the relativistic increase in plasma wavelength) will be

$$\mathcal{E} \approx 2\gamma_p^2 (E_{\max}/E_0) m_e c^2. \quad (1)$$

In this paper, we explore both the SMWF and FLW regimes for the generation of relativistic electrons. In the SMWF regime we show that the acceleration of energetic electrons is initiated by the plasma wave generation due to a Raman scattering instability. Increasing the growth rate of the instability sufficiently, results in wavebreaking of the plasma wave, with a large associated current of accelerated electrons. By retaining a similar laser power but reducing the pulse length dramatically we are able to access the FLW regime. In this regime no modulation of the laser pulse at the plasma frequency is observed. However, the breaking of a large amplitude plasma wave is still witnessed. Indeed the maximum energy of detected electrons is significantly greater, suggesting the growth of plasma waves with peak amplitude greater than the initial plasma density. Because in this regime, the interaction of the plasma wave and the electrons trapped by it with the laser pulse is minimized, the electron beam is found to have improved quality compared to that produced in the SMWF regime.

II. EXPERIMENTAL PARAMETERS AND SET-UP

The results described in this paper were obtained from a series of experiments performed at the Rutherford–Appleton Laboratory with the Vulcan:CPA laser,¹⁸ and at the Laboratoire d'Optique Appliquée with the Salle Jaune laser.¹⁹ The Vulcan:CPA laser generated laser pulses with up to 50 J on target in a 1 ps pulse. Wavefront distortion in the beam due to thermal lensing in the amplifiers is corrected with a static adaptive optic. This allows the beam to be focused to a roughly 3 times diffraction limited spot. In the experiments detailed here the laser beam was focused to a $10 \mu\text{m}$ spot diameter (FWHM), resulting in intensities $I > 10^{19} \text{ W cm}^{-2}$, when focused in vacuum. The Salle Jaune laser has a maximum energy on target of about 1 J, but this coupled with a 30 fs pulse length, results in similar laser powers of greater than 30 TW. For these experiments it was found that increasing the focusing length increased the electron beam quality. A 1 m focal length parabolic mirror was used, which resulted in a focal spot of $18 \mu\text{m}$ waist, giving focused intensities in vacuum of around $3 \times 10^{18} \text{ W cm}^{-2}$.

To prevent ionization defocusing of the laser beam before reaching focus, the laser beam was always focused on the edge of a high-density gradient gas-jet. The density pro-

file of the nozzle had been previously measured by interferometry. The nozzle has been optimised to ensure that the vacuum-gas interface is as sharp as possible while retaining a flat density profile within the gas itself.²⁰ The density of neutrals was varied by varying the backing pressure on the jet. Hydrogen or helium were generally used in these experiments, which ensures that the plasma density produced remains uniform, without the intensity dependant ionization profile that characterizes the interaction with other gases at these laser intensities. This also ensures that the gas jet is free from cluster formation. The gas jet densities measured in these experiments were consistent with the full ionization of the neutrals (2 electrons per molecule) as measured by interferometry.

The spectrum of the beam transmitted through the gas jet was attenuated by reflecting off a glass plate, before directing it out of the vacuum chamber. The collection angle of the transmitted beam was comparable to that of the incoming beam. The beam was focused into a spectrometer and the spectrum detected with a 16-bit (high dynamic range) CCD camera. The spectral response of the system was calibrated with a black-body emitter placed at the focal plane of the laser beam. The glass plate for collecting the transmitted light had a small hole ($\phi=1$ cm) in it to allow energetic electrons to pass through without scattering or energy loss. The electrons were then collimated (using an aperture in a lead piece) before passing into the electron spectrometer. Typically the collimator has a collection angle $\sim f/100$. The electrons were dispersed in the spectrometer by use of an electromagnet. The electromagnet used has specially shaped pole pieces to allow imaging in the spectral plane of the electron source. The magnetic field of the electromagnet, and hence the dispersion of the spectrometer, can be altered by changing the current passing through its solenoidal coils. This allows the same instrument to measure a wide range of energies on a series of shots with different current settings. Hence the spectrometer can be used in imaging mode for energies of 0 to 217 MeV. The dispersed electrons were detected with silicon barrier detectors (of circular area ≈ 1 cm² each). The detectors were biased, and the current generated by ionizing radiation in the diodes depletion region measured on oscilloscopes. To measure the background signal due to x-ray generation, diodes were placed at the same angle but out of the plane of the electron dispersion. Additional divergence measurements were made by using stacks of radiochromic film (RCF) spaced by copper pieces of known thickness. The stack was placed 5 cm after the laser focus. RCF has a calibrated response to the dose of ionizing radiation passing through it. The beam profiles thus obtained were corrected for scattering and x-ray generation by use of a tracking code.²¹

III. SELF-MODULATED WAKEFIELD

Figure 1 shows the spectra of the transmitted light when laser pulses from Vulcan ($\tau_l \sim 1$ ps) were passed through a gas jet for two different plasma densities, $n_e = 4 \times 10^{18}$ cm⁻³ and $n_e = 7.5 \times 10^{18}$ cm⁻³. In both cases the pulse length is long relative to the plasma wave length. Fig-

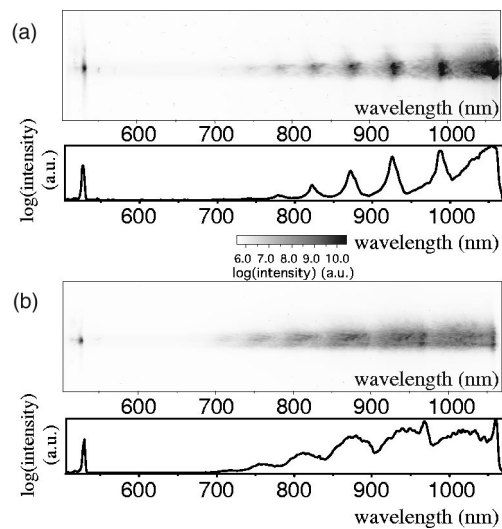


FIG. 1. Transmitted beam spectra with (a) $n_e = 4 \times 10^{18}$ cm⁻³ and $I = 2 \times 10^{19}$ W cm⁻² and (b) $n_e = 7.5 \times 10^{18}$ cm⁻³ and $I = 1 \times 10^{19}$ W cm⁻².

ure 1(a) shows up to 8 satellite frequencies of the transmitted light on the blue-shifted side of the fundamental laser frequency, plotted as $\log(\text{intensity})$. The satellites are clearly differentiated from one another, and are spaced by constant intervals of the plasma frequency ω_p . The spectrum has a similar character on the red side of the fundamental. One can see obviously the analogy to Raman scattering from molecules. However, one basic difference exists between plasma Raman scattering and molecular Raman scattering, and that is the excitation of the plasma wave. The plasmons that constitute the plasma wave are not fixed quantum states. As the plasma wave grows to large amplitude, in particular when the plasma wave amplitude $\delta n/n_0 \sim 1$, then the plasma wave can no longer be described as a linear oscillation at frequency ω_p . Indeed the density peaks become steepened. This nonlinear plasma wave can be Fourier-decomposed into its harmonic constituents as follows: $(n^m/n_0) = (m^m/(2^{m-1}m!)) \cdot (\delta n/n_0)^m$, where n^m is the amplitude of the m -th harmonic of the plasma wave of peak amplitude $\delta n/n_0$. One can therefore see why sidebands are so efficiently generated even though the growth of the FRS predicts that in 1 ps there is only enough time for the first electromagnetic sideband to grow to large amplitude. Evidently the cascading is due to scattering from the nonlinear steepened plasma wave, rather than a step-wise scattering of the successive electromagnetic sidebands off a linear plasma wave (i.e., one that has a harmonic content only at ω_p).

Increasing the growth of the plasma wave by further increasing the FRS growth rate, cannot lead to an indefinitely increasing plasma wave amplitude, due to the wavebreaking limit. Mori *et al.* have derived the spatio-temporal growth rates for the FRS instability in the relativistic regime (i.e., $a_0 > 1$).⁵ They find that the FRS growth rate saturates with intensity and in this regime one can only achieve further plasma wave growth by its dependence on density. This is shown in Fig. 1(b), where a higher density is used compared to Fig. 1(a). The sidebands can still be discerned in this figure, with a slightly greater wavelength separation since ω_p

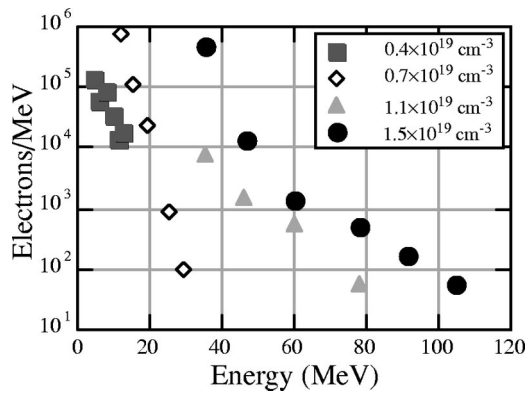


FIG. 2. Electron spectra from SMWF for a variety of different densities.

$\propto \sqrt{n_e}$. However, the sidebands are noticeably broader. This is though the interaction length is the same as before. This increased width suggests that the scattering plasma wave is losing coherence.

The reason for this loss of coherence is demonstrated by the spectrum of electrons accelerated by the generated plasma wave, shown in Fig. 2. The figure shows that even at $n_e = 4 \times 10^{18} \text{ cm}^{-3}$, when the plasma wave is still coherent, there are a significant number of electrons accelerated to quite high energy (up to 13 MeV before the number falls below the detection threshold). These trapped electrons are from the tail of the hot temperature distribution, demonstrating that these plasmas can reach extremely high temperatures due to other parametric instabilities.²² In the large electric fields of the plasma wave, it is possible to further accelerate these electrons to high energies. But one can see by their modest energies in comparison to Eq. (1) that the associated electric field of the plasma wave is still less than E_{wb} . An estimate of the plasma wave amplitude from both the maximum energy and Raman satellite amplitudes gives $\delta n/n_0 \approx 0.1$ for this density.

However, one can see that as the density is increased to $n_e = 7.5 \times 10^{18} \text{ cm}^{-3}$, the number and maximum energy of the electrons increases markedly. This is even more pronounced as the plasma wave growth rate is increased by increasing the density further. Not only is the maximum energy of the electron distribution increased, but there is a significant tail to the distribution that can no longer be fitted by a single Maxwellian distribution. Divergence measurements have also been performed using nuclear activation techniques.²³ Taking account for the beam divergence, one finds upwards of 10^{12} relativistic electrons in total generated by this interaction, i.e., practically all the electrons from within the focal volume over a Rayleigh length. Clearly, such a huge fraction of accelerated electrons cannot be simply explained by the trapping of hot electrons. The accelerated electrons are generated by wavebreaking. As described above, charge sheets in opposite halves of the plasma wave oscillation can cross longitudinally, so that instead of feeling a returning force, some of the electrons, those traveling in the same direction as the phase velocity of the plasma wave, can feel a continuous acceleration in the direction in which they were traveling. This of course also destroys the coher-

ence of the plasma wave. Hence the broadening of the satellites in the transmitted spectra is a clear signature of the onset of wavebreaking. At higher densities, the broadening is so severe that it becomes difficult to distinguish the individual satellites. Note also that there is clear evidence of the increased growth of the FRS at higher density from Fig. 1(a) to Fig. 1(b) even though the intensity of the second shot was slightly lower. This reiterates the weak dependence of the FRS growth rates on intensity in this regime.

A further increase in density in Fig. 2 shows that the maximum energy of accelerated electron approaches 100 MeV. From Eq. (1), for this density ($n_e = 1.5 \times 10^{19} \text{ W cm}^{-2}$) for which $\gamma_p \approx 8$, the maximum expected energy would be $\mathcal{E}_{\max} \approx 130(\delta n/n_0)$, suggesting that $\delta n/n_0$ is very close to 1. However, both simulation and experiment^{24–28} of these interactions have shown that in the SMWF regime, severe wavebreaking and heating by other parametric instabilities limits the wavebreaking amplitude of the plasma wave to $\delta n/n_0 < 0.4$. The simulations show that such high energies are produced due to secondary processes, either self-generated fields due to the high current bunch of electrons²⁷ or due to a direct resonant interaction with the laser beam.²⁸ As a result of these secondary processes, and the loss of coherence of the plasma wave, it is found that the emitted beam has a reasonably high divergence (for example, 20 MeV electrons have a divergence of $>12^\circ$ FWHM), which is comparable to the initial laser divergence.²³ This obviously has implications for the emittance of electron beams produced by this method.

IV. FORCED LASER WAKEFIELD

To explore the interaction of an ultrashort laser pulse, we used the 30 fs, 1 J laser in the Salle Jaune. Both a short and long focal length parabola were used for the focusing. Results with a short focal length parabola (f 7.5) have been described previously.³² With this parabola, in the regime where $\tau_l \sim 2\pi\omega_p^{-1}$, the maximum energy gain was found to be limited by the Rayleigh length ($Z_r \sim 300 \mu\text{m}$). In this paper we report on an extension of this study performed with

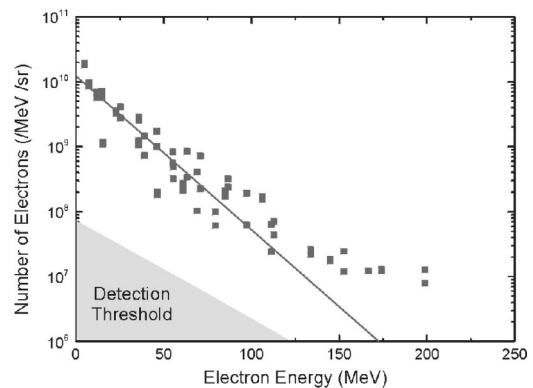


FIG. 3. Electron spectrum for $n_e = 2.5 \times 10^{19} \text{ cm}^{-3}$ (squares) from FLW. An effective electron temperature of $(18 \pm 1) \text{ MeV}$ is obtained from an exponential fit for $\mathcal{E} < 130 \text{ MeV}$ (continuous line). The measurement is averaged over the $f/100$ opening of the spectrometer and the detection threshold was chosen for a signal-to-noise-ratio of 25:1.

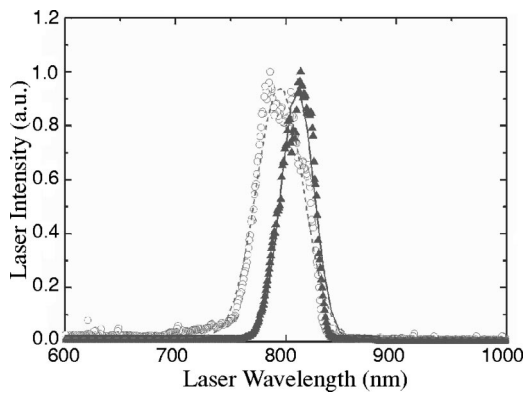


FIG. 4. Spectrum of the laser beam in vacuum (triangles and solid line) and after transmission through the plasma (circles and dashed line) in the FLW regime. The spectrum is broadened from an initial 33 nm to 48 nm. NB: there is no signature of satellite frequencies, as seen in the SMWF.

a $f = 1$ m parabola. This gives an $a_0 \sim 1.2$. For plasma wave growth in the nonlinear wakefield regime, this should not be large enough to enable us to reach the cold wavebreaking limit. However, when the laser is focused on the edge of a gas jet of density $n_e \approx 2.5 \times 10^{19} \text{ W cm}^{-2}$, one obtains the electron spectrum shown in Fig. 3. A large current of accelerated electrons is once again produced (total charge > 5 nC), now with a maximum in energy beyond 200 MeV. This is despite the reduction of more than $50\times$ in laser energy compared to the spectra shown in Fig. 2 in the SMWF regime. Divergence measurements show that the highest energy electrons are well collimated ($< 2^\circ$ for > 50 MeV electrons). Once again wavebreaking of a relativistic plasma wave is responsible for this current of energetic electrons. Indeed, the reduced divergence compared to the SMWF regime demonstrates that the electrons are purely accelerated by the plasma wave, and that the effect of direct laser acceleration is minimal.²⁸ Also improved is the shot-to-shot variation in this regime. (Though the electron charge for a given energy does show a shot-to-shot variation, typically by a factor of 2–3.) This is a considerable improvement on

SMWF experiments where this can be greater than an order of magnitude.²⁹ This is likely to be because the FLW is less dependent on fast growth of instabilities from noise sources.

Transmitted spectra are shown in Fig. 4, from which a broadening of the transmitted spectra is evident. However, noticeably, there is a complete absence of satellites. Evidently the pulse is not modulated at the plasma frequency, though it is likely to have experienced a compression due to the effects of ionization and the growth of a preceding plasma wave due to snow-ploughing of electrons in front of the laser.

The main features of nonlinear wakefield generation by an ultrashort pulse are demonstrated through the use of particle-in-cell (PIC) simulations, as shown in Fig. 5. These simulations were performed using the code OSIRIS.³³ Most noticeably the pulse (on the left) quickly develops from a symmetric profile to one which has an increasingly sharp rising edge. This is due to the effect of plasma wave growth (on the right). An initially nonlinearly steepened plasma wave is generated, as shown by the characteristic saw-tooth associated E-field. However, apart from the first bucket, the wake quickly disappears as it is driven to very high amplitude ($E \sim 1 \text{ TV m}^{-1}$). This is due to the effect of wavebreaking which takes most of the energy out of the wake. The laser field at this time is observed to have an extremely sharp rising edge, which can continue to drive the first trailing bucket of the plasma wave even after wavebreaking. However, to see these effects one requires an initial $a_0 > 2$. Repeating the simulations for $a_0 \sim 1.2$, though generating a large amplitude wakefield, never exhibits wavebreaking. Also in the one-dimensional (1-D) description, one can see that a measurable amount of light is trapped in front of the sharp edge and is gradually redshifted as it loses energy to the plasma wave. This is shown more clearly in Fig. 6, which shows the spectrum of the laser pulse at early and late times in the simulation. This figure shows a blue-shifting of the peak of the spectrum as seen in the experiment (Fig. 3) due to compression by the plasma wave. However, the redshifted tail to the spectrum obtained in the simulation is absent in the

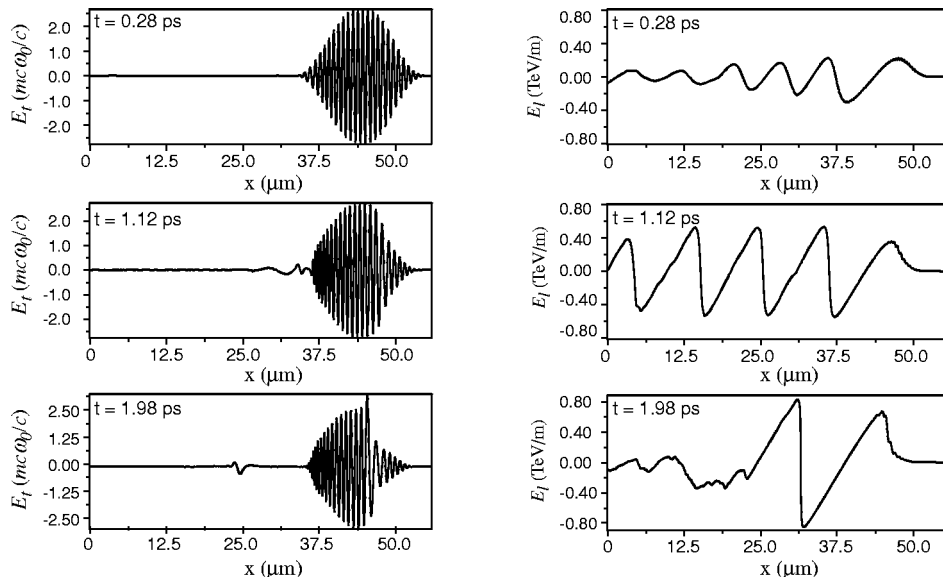


FIG. 5. 1-D PIC simulation results of a nonlinear wakefield showing laser pulse shape E_L and plasma wave E-field E_1 at 3 different times $a_0 = 3$ pulse traveling in $n_e = 2 \times 10^{19} \text{ cm}^{-3}$.

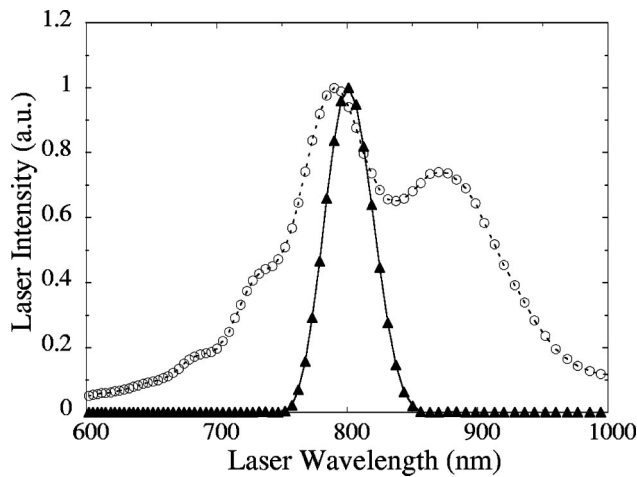


FIG. 6. Spectrum of the laser beam obtained from a 1-D simulation after $t = 0.28$ ps (triangles and solid line) and $t = 1.98$ ps (circles and dashed line) in the FLW regime.

experimental spectrum. Though the 1-D simulations provide qualitative information about the interaction, to fully understand the FLW regime one must perform 3-D simulations.¹³

In these 3-D simulations, despite being in the short pulse regime ($\tau_l \sim 2\pi\omega_p^{-1}$), self-focusing of the laser energy is observed. This can explain how the intensity can be sufficiently high for an impulsive plasma wave growth to wave breaking amplitude, despite the fact that neither the initial laser intensity nor the observed pulse compression are sufficiently large. At lower densities, including at the wakefield resonant density $\tau_l = \pi\omega_p^{-1}$, no accelerated electrons are observed at all. Hence one can see that there is a subtle difference between the Forced Laser Wakefield and nonlinear wakefield regimes. Without self-focusing, no wavebreaking is observed, but this can only happen if the pulse length is not too short initially (i.e., $\tau_l < \pi\omega_p^{-1}$). But if there is self-focusing then pulse erosion takes place, which can allow efficient wake generation. Since the very front of the pulse is not self-focused, the erosion will be more severe, explaining why the redshifted front edge seen in the 1D simulations is not observed in the experiment. In fact, ionization, which is not included in this model, further enhances this effect by increasing diffraction of the front of the pulse. The wake then is mostly formed by this fast rising edge, and the back of the pulse has little interaction with the relativistic longitudinal oscillation of the plasma wave electrons. Indeed the increase of plasma wave length due to relativistic effects means that the breaking and accelerating peak of the plasma wave sits behind most, if not all, of the laser pulse. Hence its interaction and that of the accelerated electrons with the laser pulse is minimized, thus reducing emittance growth due to direct laser acceleration. Indeed the emittance measured from this experiment for high energy electrons [$\epsilon_n = (2.7 \pm 0.9)$ π mm mrad for $\mathcal{E} = (55 \pm 2)$ MeV] has been found to be comparable if not better than modern LINACs.²¹

Also observed in the 3-D simulations is that the radial plasma wave oscillations interact coherently with the longitudinal field, so enhancing the peak amplitude of the plasma wave. This coupled with the aforementioned strong self-

focusing are ingredients absent from one-dimensional treatments of this interaction. Even in 2-D simulation, it is not possible to observe electrons beyond 200 MeV, as measured in this experiment, since except in 3-D simulations, both the radial plasma wave enhancement and self-focusing effects are underestimated. Hence it is only in 3-D simulations that $E_{\max} \sim E_{\text{wb}}$ can be reached.¹³ That such large electric fields are generated, demonstrates another important difference between FLW and SMWF regimes, since in the latter, plasma heating by instabilities limits the accelerating electric field to an order of magnitude below the cold wavebreaking limit. It should be noted that the electric field inferred for these FLW experiments is in excess of 1 TV m^{-1} , considerably larger than any other coherent accelerating structure created in the laboratory. In fact this figure is 4 orders of magnitude greater than the electric field strength in the state-of-the-art accelerators in use these days in high energy physics experiments.

V. DISCUSSION

We have shown that in high intensity highly nonlinear laser-induced wavebreaking interactions, it is not necessary to have a long laser pulse which self-modulates and resonantly excites the plasma wave. Nonlinear interactions, especially within the leading edge of the pulse, such as ionization, self-focusing, optical shock compression and radial plasma wave amplification, can all force a plasma wave to wavebreaking amplitude. Having an ultrashort pulse not only increases the efficiency of the interactions, but can improve the beam quality, both in energy (due to the reduced heating of the plasma and thus higher plasma wave amplitude) and in emittance (due to the reduced interaction between accelerated electrons and the laser pulse).

One interesting consequence of these extremely large amplitude plasma waves is that their wavelength $\lambda_{\text{NL}} = (2/\pi)(1 + (a_0^2/2))^{1/2}\lambda_p$ increases. Hence one can consider wakefield by lasers with otherwise undesirably long pulse lengths, by increasing their focused intensity. This will make it possible to reach the FLW regime with superpowerful laser pulses now being constructed from high energy glass laser systems. Though the limited gain bandwidth of glass, typically restricts these laser pulses to $\tau_l > 300$ fs, their large size can compensate to give extremely high powers. Several facilities around the world are now being developed to reach the petawatt regime in the near future. A 2-D simulation using OSIRIS showing a petawatt laser pulse (of pulse length 300 fs) traveling in an underdense plasma is shown in Fig. 7. The petawatt laser has been focused to give $\gamma_p \approx 30$, so bringing the resonant density from around $5 \times 10^{16} \text{ cm}^{-3}$ to above $1 \times 10^{19} \text{ cm}^{-3}$, thus allowing consequently much greater electric field plasma waves to be generated. The simulation shows that the laser pulse is not greatly modified after traveling $\sim 150 \mu\text{m}$ into the plasma [Fig. 7(a)], unlike a similar pulse length but lower power interactions as shown in Sec. III and in simulation by Tzeng *et al.*⁹ However, the electric field trailing the laser pulse at the same time is again huge [Fig. 7(b)]. This results in wavebreaking as can be seen from the spectrum of electrons after a laser propagation distance of $300 \mu\text{m}$, which shows a significant number of ac-

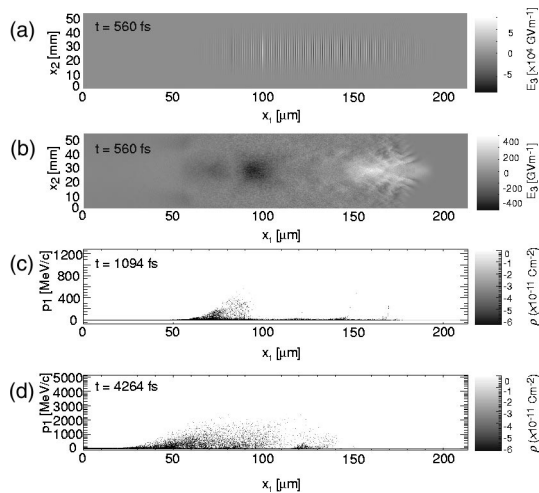


FIG. 7. Simulation showing a 1 PW, $\tau_l = 300$ fs laser traveling in $n_e = 1 \times 10^{19} \text{ cm}^{-3}$ plasma. (a) Laser field E_2 at $t = 560$ fs; (b) longitudinal E-field E_1 also $t = 560$ fs; (c) longitudinal electron momentum p_1 at $t \approx 1$ ps; and (d) p_1 at $t \approx 4$ ps.

celerated electrons trailing the laser pulse [Fig. 7(c)]. This beam of electrons continues to be accelerated until after about 4 ps of laser propagation [>1 mm—Fig. 7(d)] many have reached energy in excess of 1 GeV.

In conclusion, the comparison of SMWF and FLW regimes of self-generated relativistic electron sources has shown the improved beam characteristics in the FLW regime, with greatly reduced laser requirements. Hence, it is conceivable that the FLW accelerator will be of great interest for the applications of large energy spread electron beams that have been recently demonstrated, such as gamma-radiography³⁰ and nuclear activation.^{23,31,32} It is also conceivable that with the higher energies expected from the interaction of petawatt class laser systems, that several new applications may be considered, such as the secondary production of positrons,³⁴ pions, muons and neutrinos.^{35,36}

¹E. Esarey, P. Sprangle, J. Krall, and A. Ting, *IEEE Trans. Plasma Sci.* **24**, 252 (1996).

²T. Tajima and J. Dawson, *Phys. Rev. Lett.* **43**, 267 (1979).

³P. Sprangle, E. Esarey, A. Ting, and G. Joyce, *Appl. Phys. Lett.* **53**, 2146 (1988).

⁴N. E. Andreev, L. M. Gorbunov, V. I. Kirsanov, A. A. Pogosova, and R. R. Ramazashvili, *JETP Lett.* **55**, 571 (1992).

⁵W. B. Mori, C. D. Decker, D. E. Hinkel, and T. Katsouleas, *Phys. Rev. Lett.* **72**, 1482 (1994).

⁶J. F. Drake, P. K. Kaw, Y. C. Lee, G. Schmidt, C. S. Liu, and M. N. Rosenbluth, *Phys. Fluids* **17**, 778 (1974).

⁷D. W. Forslund, J. M. Kindel, and E. L. Lindman, *Phys. Fluids* **18**, 1002 (1975).

⁸S. V. Bulanov, I. N. Inovenkov, V. I. Kirsanov, N. M. Naumova, and A. S. Sakharov, *Phys. Fluids B* **4**, 1935 (1992).

⁹K.-C. Tzeng, W. B. Mori, and C. D. Decker, *Phys. Rev. Lett.* **76**, 3332 (1996).

¹⁰C. D. Decker, W. B. Mori, and T. Katsouleas, *Phys. Plasmas* **3**, 2047 (1996).

¹¹D. F. Gordon, B. Hafizi, P. Sprangle, R. F. Hubbard, J. R. Peñano, and W. B. Mori, *Phys. Rev. E* **64**, 046404 (2001).

¹²S. V. Bulanov, V. I. Kirsanov, and A. S. Sakharov, *JETP Lett.* **50**, 198 (1989).

¹³V. Malka, S. Fritzler, E. Lefebvre *et al.*, *Science* **298**, 1596 (2002).

¹⁴V. I. Berezhiani and I. G. Murusidze, *Phys. Lett. A* **148**, 338 (1990).

¹⁵P. Sprangle, E. Esarey, and A. Ting, *Phys. Rev. E* **41**, 4463 (1990).

¹⁶A. I. Akhiezer and R. V. Polovin, *Sov. Phys. JETP* **3**, 696 (1956).

¹⁷A. Modena, Z. Najmudin, A. E. Dangor, C. E. Clayton, K. A. Marsh, C. Joshi, V. Malka, C. B. Darrow, C. Danson, D. Neely, and F. N. Walsh, *Nature (London)* **377**, 606 (1995).

¹⁸C. N. Danson, J. Collier, D. Neely *et al.*, *J. Mod. Opt.* **45**, 1653 (1998).

¹⁹M. Pittman, S. Ferre, J. P. Rousseau, L. Notebaert, J. P. Chambaret, and G. Cheriaux, *Appl. Phys. B: Lasers Opt.* **74**, 529 (2002).

²⁰V. Malka, C. Coulaud, J. P. Geindre, V. Lopez, Z. Najmudin, D. Neely, and F. Amiranoff, *Rev. Sci. Instrum.* **71**, 2329 (2000).

²¹S. Fritzler, V. Malka, E. Lefebvre *et al.*, "Beam quality studies for the laser-plasma concept," submitted to *Phys. Rev. Lett.*

²²K.-C. Tzeng and W. B. Mori, *Phys. Rev. Lett.* **81**, 104 (1998).

²³M. I. K. Santala, Z. Najmudin, E. L. Clark, M. Tatarakis, K. Krushelnick, A. E. Dangor, V. Malka, J. Faure, R. Allott, and R. J. Clarke, *Phys. Rev. Lett.* **86**, 1227 (2001).

²⁴C. E. Clayton, K.-C. Tzeng, D. Gordon, P. Muggli, W. B. Mori, C. Joshi, V. Malka, Z. Najmudin, A. Modena, D. Neely, and A. E. Dangor, *Phys. Rev. Lett.* **81**, 100 (1998).

²⁵A. Ting, K. Krushelnick, C. I. Moore, H. R. Burris, E. Esarey, J. Krall, and P. Sprangle, *Phys. Rev. Lett.* **77**, 5377 (1996).

²⁶S. P. Le Blanc, M. C. Downer, R. Wagner, S. Y. Chen, A. Maksimchuk, G. Mourou, and D. Umstadter, *Phys. Rev. Lett.* **77**, 5381 (1996).

²⁷D. Gordon, K. C. Tzeng, C. E. Clayton, A. E. Dangor, V. Malka, K. A. Marsh, A. Modena, W. B. Mori, P. Muggli, Z. Najmudin, D. Neely, C. Danson, and C. Joshi, *Phys. Rev. Lett.* **80**, 2133 (1998).

²⁸A. Pukhov, Z.-M. Zheng, and J. Meyer-ter-Vehn, *Phys. Plasmas* **6**, 2847 (1999).

²⁹Z. Najmudin, A. E. Dangor, A. Modena *et al.*, *IEEE Trans. Plasma Sci.* **28**, 1057 (2000).

³⁰R. D. Edwards, M. A. Sinclair, T. J. Goldsack *et al.*, *Appl. Phys. Lett.* **80**, 2129 (2002).

³¹W. P. Leemans, D. Rodgers, P. E. Catravas, C. G. R. Geddes, G. Fubiani, E. Esarey, B. A. Shadwick, R. Donahue, and A. Smith, *Phys. Plasmas* **8**, 2510 (2001).

³²V. Malka, J. Faure, J. R. Marques, F. Amiranoff, J. P. Rousseau, S. Ranc, J. P. Chambaret, Z. Najmudin, B. Walton, P. Mora, and A. Solodov, *Phys. Plasmas* **8**, 2605 (2001).

³³R. G. Hemker, Ph.D. thesis, University of California, Los Angeles, 2000.

³⁴C. Gahn, G. D. Tsakiris, G. Pretzler, K. J. Witte, P. Thirolf, D. Habs, C. Delfin, and C. G. Wahlstrom, *Phys. Plasmas* **9**, 987 (2002).

³⁵S. Karsch, D. Habs, T. Schatz, U. Schramm, P. G. Thirolf, J. Meyer-ter-Vehn, and A. Pukhov, *Laser Part. Beams* **17**, 565 (1999).

³⁶D. Umstadter, *Phys. Plasmas* **8**, 1774 (2001).